GENERALIZED VISCOUS VORTEX MODEL FOR APPLICATION TO FREE-VORTEX WAKE AND AEROACOUSTIC CALCULATIONS

Mahendra J. Bhagwat* J. Gordon Leishman†

Alfred Gessow Rotorcraft Center,
Department of Aerospace Engineering,
Glenn L. Martin Institute of Technology,
University of Maryland, College Park, Maryland 20742

Abstract

The development of a generalized viscous vortex model is described for application in rotor aeroacoustic analyses. A brief summary is given of previous models for the viscous core growth and induced velocity field of a trailing tip vortex. The assumptions made for the vortex core growth are shown to influence the predictions of the rotor wake geometry, as well as the induced velocities, airloads, and performance, thereby emphasizing the need for a more universal and physically representative vortex model. In the present approach, the viscous core growth was modeled using an extension of the classic Lamb-Oseen model for the diffusion of laminar vortices. Turbulence in the tip vortex affects the diffusion of vorticity, and these effects were incorporated using an empirically validated correction for the average apparent or "eddy" viscosity. The vortex induced velocity profiles measured in experiments were found to exhibit strong self-similarity when using the vortex core radius as a length-scale, suggesting that a generalized model is possible. A family of algebraic models for the swirl, axial, and radial components of the velocity induced by a viscous trailing tip vortex is proposed. These velocity components were found from a solution to a simplified form of the incompressible Navier-Stokes equations. The velocity profiles are written in terms of a single integer exponent with the viscous core growth being given by a semi-empirical relation for the turbulent viscosity that scales as a function of the vortex Reynolds number. The model is compared with velocity field measurements for both fixed-wing and rotating-wing tip vortices, with good agreement.

Nomenclature

a_1	Squire's parameter
b_1	Non-dimensional vortex core growth rate
c	Wing chord, m
C_{d_0}	Zero-lift drag coefficient
D_0	Zero-lift drag of wing
$\overline{d}$	Non-dimensional distance, $= z\Gamma_v/(V_\infty c^2)$
n	Integer parameter
N_b	Number of blades
p	Static pressure, Pa
P_0	Profile power coefficient, W
R	Rotor radius, m
r, θ, z	Cylindrical coordinate system, (m, rad, m)
$\overline{r}$	Non-dimensional radial distance, $= r/r_c$
r_c	Vortex core radius, m
r_{c_0}	Initial vortex core radius, m
Re	Chord Reynolds number, $= V_\infty c/\nu$
Re_v	Vortex Reynolds number, $= \Gamma_v/\nu$
t	Time, s
$\overline{V}$	Non-dimensional peak velocity, $= V_{\theta_{max}} c/\Gamma_v$
V_∞	Free-stream velocity, m s^{-1}
V_r	Vortex induced radial velocity, m s^{-1}
V_θ	Vortex induced swirl (tangential) velocity, m s^{-1}
$V_{\theta_{max}}$	Maximum swirl (tangential) velocity, m s^{-1}
V_z	Vortex induced axial velocity, m s^{-1}
z_0	Effective origin, m
α	Oseen parameter $= 1.25643$
$\overline{\Gamma}$	Non-dimensional circulation, $= \Gamma/(\Omega R c)$
Γ_v	Net vortex circulation, m^2 s^{-1}
δ	Eddy viscosity coefficient
ε	Small number
ν	Kinematic viscosity, m^2 s^{-1}
Ω	Rotor rotational frequency, rad s^{-1}
ρ	Density, kg m^{-3}
ζ	Wake age, deg
ζ_0	Virtual origin in wake age, deg

Abbreviations

BVI	Blade Vortex Interaction
TPP	Tip-Path-Plane

* Graduate Research Assistant. Currently Aerospace Engineer, Advanced Rotorcraft Technology, Inc., Mountain View, California.

† Professor.

Presented at the 58th Annual Forum and Technology Display of the American Helicopter Society International, Montréal, Canada, June 11–13, 2002.

Introduction

Modeling the viscous core structure and temporal development of lift-generated trailing vortices has been a continuing challenge in both fixed-wing and rotating-wing aerodynamic problems. The persistence of aircraft tip vortices poses a wake-hazard problem for any following aircraft, and this is a major factor limiting the capacity of large airports – e.g., see Ref. 1. The prediction of the induced velocities and strength (circulation) history of the tip vortices as they trail behind an aircraft has been the subject of much research over the past five decades (e.g., see Refs. 2–8). However, the properties of the vortex, such as its laminar or turbulent core structure and its related diffusive and dissipative characteristics, are still not well understood. In depth reviews of these problems have been presented in Refs. 5 & 8.

For rotating-wing aircraft, the blade tip vortex characteristics have an even more significant impact on rotor airloads and performance because of their close proximity to the rotating blades. Therefore, an improved modeling capability for the tip vortices directly translates into improved predictions of blade loads, rotor performance, and rotor acoustics (Ref. 9). However, because of the inherent difficulties in performing detailed vortex flow measurements in rotor wakes, rotating-wing analyses have depended heavily on the use of fixed-wing measurements for the development of empirical vortex models (Ref. 10).

The increasingly routine use of free-vortex wake models in rotating-wing aeroacoustic analyses further highlights the importance of more accurately modeling the viscous nature of the tip vortex structures. Although these free-vortex wake models are based on potential flow theory, the formation of the wake behind any lifting surface must be considered as a viscous phenomenon. Therefore, most free-vortex wake models include semi-empirical models for the tip vortex core structure and also, possibly, the viscous growth of the vortex core (e.g., Refs. 11–13). The rotor induced velocity predictions are, in general, sensitive to these parameters, but applications that focus on modeling close interactions between the tip vortices and the rotor blades (blade vortex interactions or BVIs) make it even more essential to properly represent the tip vortex core structures. Gandhi & Tauszig (Ref. 14) have shown the sensitivity of the viscous core models on BVI prediction, and have stressed the need to properly resolve such vortex modeling issues.

A complete description of a viscous, turbulent, trailing vortex requires solution to the full Navier-Stokes equations. Analytical solutions to these non-linear sets of equations is not possible, whereas numerical solutions are deterred by formidable computational costs as well as building satisfactory turbulence models. Closed-form solutions for vortex flows can only be obtained by further simplifying the governing equations, e.g., Refs. 15–18. Several semi-empirical models have been developed, e.g., Refs. 19–22, and have been applied to the modeling of trailing vortices with generally good results. The strongly self-similar structure of the tip vortices suggests a further simplification based on the assumption of an axisymmetric flow. The vortex length scale dictated by the viscous core radius can then be modeled empirically, and independently from the representation of the velocity profile.

A common approach is to represent the induced velocity using a desingularized algebraic profile, with a constant viscous core size or a diffusive core growth with time that is based on the Lamb-Oseen model. Algebraic models for the vortex induced velocity profiles are popular in engineering applications because of their simplicity and computational efficiency. One of the most commonly used models is the algebraic model suggested by Scully & Sullivan (Ref. 19) and also by Kaufmann (Ref. 20). This model qualitatively predicts the overall velocity distribution, but when compared to both fixed-wing and rotating-wing measurements the model tends to underpredict the peak swirl velocity (Ref. 23). A family of algebraic vortex-induced velocity models was proposed by Vatistas (Ref. 21), which showed a good comparison with the measured swirl velocities (Refs. 23–25). The success of these algebraic models in predicting vortex induced velocity field was one motivation for the development of the present model, which extends Vatistas's approach to trailing vortices.

The present article first reviews various models for the trailing vortex structure, and then proposes a new semi-empirical model suitable for free-vortex rotor wake applications and other aeroacoustic calculations. The viscous core growth is modeled using an extension of the Lamb-Oseen model, with the effects of turbulence on the diffusive characteristics of the vortex being modeled empirically. The swirl velocity profile is identical to that given by Vatistas (Ref. 21), which is found to agree with experimental measurements. With this extended core growth model and the assumption of a swirl-velocity profile, the radial and axial velocities are solved as a solution to a simplified form of the Navier-Stokes equations. The derived models showed good comparisons with trailing tip vortex measurements for both fixed-wings and rotating-wings.

Previous Formulations

The simplest model for the swirl velocity inside a viscous vortex with a finite core is due to Rankine (Ref. 26). This model exhibits the key features of a viscous core, that is a solid-body like rotation near the vortex center and a free (potential) vortex away from the center, i.e.,

$$V_\theta(\bar{r}) = \begin{cases} \left(\dfrac{\Gamma_v}{2\pi r_c}\right)\bar{r}, & 0 \le \bar{r} \le 1, \\ \left(\dfrac{\Gamma_v}{2\pi r_c}\right)\dfrac{1}{\bar{r}}, & \bar{r} > 1. \end{cases} \quad (1)$$

where $\bar{r} = r/r_c$ is the non-dimensional radial location normalized by the viscous core radius, r_c. The viscous core radius, by definition, is the radial distance from the vortex axis to the position of the maximum swirl velocity. It must be noted that for this Rankine vortex model, the swirl velocity and vorticity distributions are discontinuous at the vortex core boundary – see Fig. 1.

The Kaufmann vortex (Ref. 20), which is more well-known as the "Scully model" (Refs. 19, 27), overcomes the singular nature of the Rankine vortex by using an algebraic velocity profile of the form

$$V_\theta(r) = \frac{\Gamma}{2\pi}\left(\frac{r}{r_c^2 + r^2}\right) \quad (2)$$

with r_c as the vortex core radius. In non-dimensional terms this desingularized model can be written as

$$V_\theta(\bar{r}) = \frac{\Gamma}{2\pi r_c}\left(\frac{\bar{r}}{1+\bar{r}^2}\right) \quad (3)$$

which reduces the maximum swirl velocity to half the value given by the Rankine model.

Vatistas (Ref. 21) also proposed a family of desingularized algebraic swirl-velocity profile for stationary vortices, which can be written in the form

$$V_\theta(r) = \frac{\Gamma_v}{2\pi}\left\{\frac{r}{\left(r_c^{2n} + r^{2n}\right)^{1/n}}\right\} \quad (4)$$

or in non-dimensional form

$$V_\theta(\bar{r}) = \frac{\Gamma_v}{2\pi r_c}\left\{\frac{\bar{r}}{\left(1+\bar{r}^{2n}\right)^{1/n}}\right\} \quad (5)$$

For the case of $n = 2$ this particular velocity profile was found to provide good agreement with measured velocities in rotor tip vortices (Refs. 23–25). It is interesting to notice that the Vatistas model with $n = 1$ corresponds to the Kaufmann or Scully model, whereas as $n \to \infty$ this model corresponds to the Rankine vortex. For $n = 2$, the model is a close approximation to the Lamb-Oseen model (see next). These desingularized algebraic models are compared in Fig. 1.

Another vortex model given by Lamb (Ref. 15) and also by Oseen (Ref. 28), is a solution to the one-dimensional laminar Navier-Stokes equations, i.e., an axisymmetric solution for the swirl velocity with the assumption that the axial and radial velocities are zero. The Lamb-Oseen vortex model for the swirl velocity is

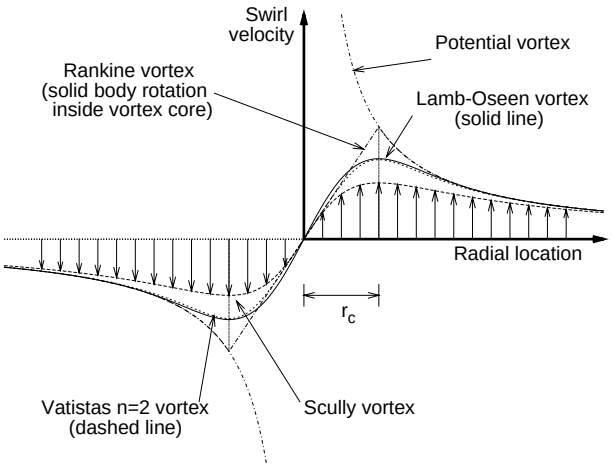

Figure 1: Distribution of induced swirl velocity inside a viscous vortex core on the basis of several models.

$$V_\theta(r) = \frac{\Gamma}{2\pi r}\left[1 - \exp\left(-\frac{r^2}{4\nu t}\right)\right] \quad (6)$$

The viscous core radius is the radial location where the swirl velocity is a maximum. This can be solved by differentiating the above equation with respect to r, and setting the derivative to zero. The viscous vortex core radius is then found to grow with time as

$$r_c(t) = \sqrt{4\alpha\nu t} \quad (7)$$

where the Oseen parameter has a value of $\alpha = 1.25643$. The Lamb-Oseen vortex model can now be written in non-dimensional form as

$$V_\theta(\bar{r}) = \frac{\Gamma_v}{2\pi r_c}\left(\frac{1 - e^{-\alpha\bar{r}^2}}{\bar{r}}\right)$$

or

$$\frac{V_\theta(\bar{r})}{V_{\theta_{max}}} = \frac{1 - e^{-\alpha\bar{r}^2}}{\bar{r}} \quad (8)$$

It can be seen from Fig. 1 that the swirl velocity given by the Vatistas $n = 2$ vortex model closely resembles that of the Lamb-Oseen vortex, i.e., it is an algebraic approximation to the one-dimensional Navier-Stokes solution. The commonly used Scully or Kaufmann model is also an algebraic approximation to the Lamb-Oseen vortex. Using a vortex length scale of $r_c = \sqrt{4\nu t}$, the Lamb-Oseen vortex model (Eq. 6) can be written as a function of the non-dimensional radial distance $\bar{r} = r/r_c$

$$V_\theta(\bar{r}) = \frac{\Gamma}{2\pi r_c \bar{r}}\left[1 - e^{-\bar{r}^2}\right] \quad (9)$$

Using a series expansion for the exponential term and ignoring higher order terms, it can be shown that

$$V_\theta(\bar{r}) = \frac{\Gamma}{2\pi r_c \bar{r}}\left[1 - \frac{1}{1+\bar{r}^2+\frac{\bar{r}^4}{2}+\cdots}\right] \approx \frac{\Gamma}{2\pi r_c}\left(\frac{\bar{r}}{1+\bar{r}^2}\right) \quad \text{for small } \bar{r} \qquad (10)$$

which is the vortex model given by Eq. 3.

The Lamb-Oseen vortex model is a time-dependent solution for a one-dimensional (axisymmetric) vortex flow. Squire (Ref. 3) showed that the solution for a trailing vortex is identical to the Lamb-Oseen solution with the axial direction, downstream from the origin of the vortex, z, being related to time as $t = z/V_\infty$. He further proposed inclusion of an average apparent or "eddy" viscosity ($\delta\nu$) in the Lamb-Oseen model to account for effects of turbulence generation on the enhanced diffusion of vorticity. An effective origin offset, z_0, was also proposed to give a finite vortex core at the origin of the trailing vortex at the generating wing. Therefore, in light of this the vortex core radius can be written as

$$r_c(t) = \sqrt{4\alpha\delta\nu\left(\frac{z+z_0}{V_\infty}\right)} \qquad (11)$$

In the case of a rotor, where the wake age $\zeta = \Omega t$, the core radius can be modeled using

$$r_c(\zeta) = \sqrt{4\alpha\delta\nu\left(\frac{\zeta+\zeta_0}{\Omega}\right)} \equiv \sqrt{r_{c_0}^2 + \frac{4\alpha\delta\nu\zeta}{\Omega}} \qquad (12)$$

In this case the time ordinate-shift, ζ_0, is responsible for the non-zero effective core radius, r_0 at the tip vortex origin where $\zeta = 0^\circ$ and, therefore, gives a more physically correct finite velocity there.

Squire hypothesized that the "eddy" viscosity is proportional to the vortex circulation strength. The eddy viscosity coefficient was then formulated in terms of the vortex Reynolds number $\left(Re_\nu \equiv \Gamma_\nu/\nu\right)$ as given by

$$\delta = 1 + a_1 Re_\nu \qquad (13)$$

where a_1 is a parameter that must be empirically determined from experimental measurements.

The one-dimensional Lamb-Oseen solution was also extended to three-dimensional vortex flows by Burgers (Ref. 16). The Burgers vortex model includes a swirl velocity similar to the Lamb-Oseen model, along with a linear distribution of radial velocity. However, this implies a constant axial velocity and is not consistent with experimental observations, which generally show an axial velocity deficit in the vortex core that decays rapidly with time, e.g., see Refs. 2, 25. Also, the linearly increasing radial velocity makes the model applicable to only small regions of flow near the vortex axis.

Newman (Ref. 17) derived exponential solutions for all three components of velocity in a trailing vortex by solving a simplified version of the three-dimensional incompressible Navier-Stokes equations. The swirl velocity in this case is the same as that given by the Lamb-Oseen model. This model was shown to give good correlation with tip vortex measurements – e.g., see Ref. 2.

One interesting commonality in all these models is the self-similarity of the velocity field. That is, the velocity profile can be represented using a single function by appropriately scaling the distance by the vortex core radius. This self-similarity of the vortex induced velocity is also observed in experimental measurements as mentioned earlier (e.g., Ref. 18, 25). Therefore, the length scale corresponding to the vortex core radius is a very important parameter in modeling the vortex characteristics. In the present study, the core growth is represented by a model similar to that given by Eq. 11, but Squire's eddy viscosity parameter, a_1, is estimated from an assemblage of experimental measurements found in the published literature.

Effect of Viscous Core Growth on Rotor Wake Predictions

The model used to represent the viscous core growth plays a significant role in free-vortex wake predictions. Because the vortex core structure affects the local induced velocity field, both the rotor wake geometry and the blade airloads predictions are influenced by the choice of vortex core models. The assumptions made for the core growth model can be an even more important factor for higher harmonic airloads and BVI predictions, as shown in Ref. 14.

Figure 2 shows the core growth model given in Eq. 11 with values of the parameter a_1 specified to vary between 2×10^{-1} to 2×10^{-4}. Experimental measurements of the core radius for a small-scale two-bladed rotor (Ref. 25) are also shown for comparison. The results suggest that a value of $a_1 = O\left(10^{-4}\right)$ best describes the physical nature of the vortex core growth, which in case of the small-scale rotor corresponds to a value of $\delta \approx 10$. For full-scale helicopter rotors, which will have much larger values of Re_ν, the same value of a_1 would suggest that the ratio of turbulent to laminar viscosity is as high as $\delta \approx 1000$. This suggests that the turbulence generation inside the tip vortex can increase its diffusive characteristics by orders of magnitude compared to that expected on the basis of laminar diffusion alone. The effects of this parameter on predictions of wake geometry and inflow distribution is now examined.

For a hovering rotor, the tip vortices trailed into the rotor wake are relatively far apart from each other, and it

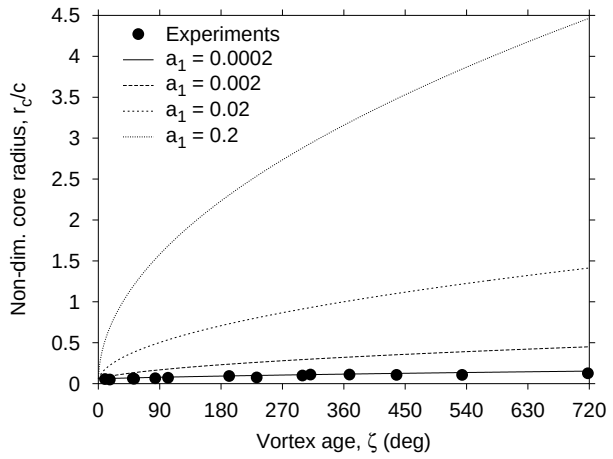

Figure 2: Vortex core growth corresponding to different values of the Squire's eddy viscosity parameter, a_1, compared with experimental results from Ref. 25.

may appear that the modeling the details of the core structure are not as significant for hovering rotor wake geometry predictions. However, this is not the case. For example, Fig. 3 shows predictions of hovering rotor wake geometry presented in the form of axial and radial tip vortex locations as a function of increasing vortex age. The predicted results are shown for different values of a_1, along with experimental results obtained with a Mach-scaled four-bladed hovering rotor, as reported in Ref. 24.

Notice that the results shown for $a_1 = 0$ correspond to pure laminar diffusion as given by the Lamb-Oseen model (see Eq. 11), i.e., where only molecular diffusion occurs. Clearly for $a_1 = O\left(10^{-1}\right)$ and $a_1 = O\left(10^{-2}\right)$, which corresponds to relatively higher rates of turbulent diffusion and a relatively fat vortex core, the axial displacements are incorrectly predicted, and the change in axial slipstream velocity at the first blade passage, in this case at $\zeta = 2\pi/N_b = 90^\circ$, is not observed. For lower values of a_1 (a correspondingly lower rate of turbulent diffusion and a smaller core size) the blade passage effect is captured properly. However, to also properly represent the radial contraction of the wake, a value as low as $a_1 = O\left(10^{-4}\right)$ was found necessary. It is interesting to notice that a laminar core growth gives excellent agreement with the observed wake geometry. This is because in hovering flight condition, there are no close interactions between the vortices and other vortices or blades.

In forward flight, the tip vortices can linger closer to the tip-path-plane (TPP) for a much longer period of time (wake age), resulting in more severe variations in local inflow and airloads, even in the absence of BVI. The effect of the vortex core growth model on the airloads was examined through a numerical experiment by examining the

(a) Axial locations of the tip vortex.

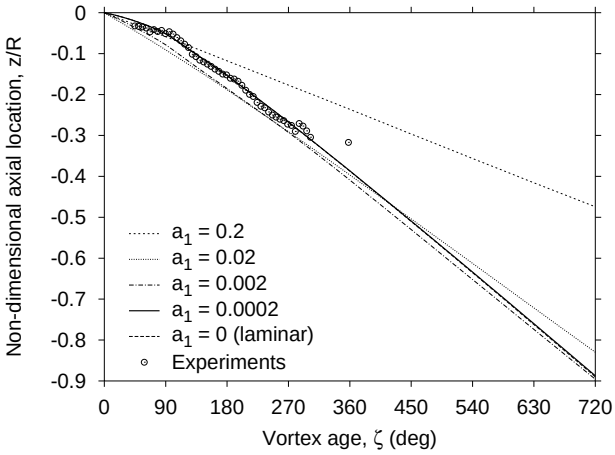

(b) Radial locations of the tip vortex.

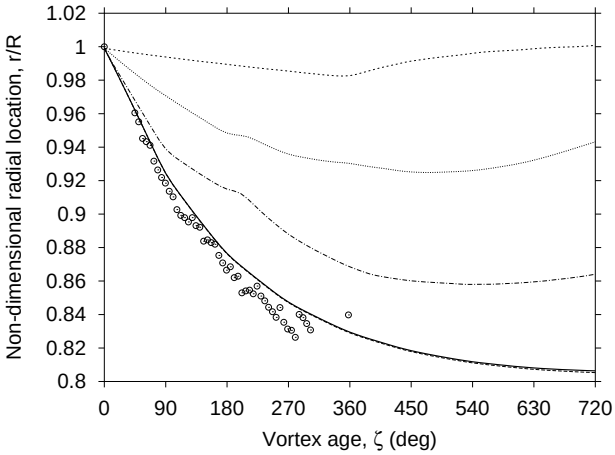

Figure 3: Effect of vortex core growth model on hovering wake geometry predictions with different values of Squire's apparent or "eddy" viscosity parameter. (a) Axial tip vortex locations as a function of vortex age. (b) Radial tip vortex locations as a function of vortex age. Experimental data from Ref. 24.

inflow distribution in the TPP for a rotor in forward flight operating at $\mu = 0.15$. The rotor shaft was tilted forward 3 degrees, and the rotor was trimmed using cyclic pitch controls to obtain zero first harmonic blade flapping with respect to the shaft. The inflow contours calculated using the free-vortex wake model are shown in Figs. 4(a)–(d). Four different values of Squire's eddy viscosity parameter, a_1, were used in the vortex model for these calculations. Each contour represents a constant value of inflow ratio, as shown in the legend of Fig. 4(d).

Notice that larger values of $a_1 = O\left(10^{-1}\right)$ (i.e., more diffused vortices) appear to mask the higher harmonic fluctuations in the inflow distribution at the rotor disk. This observation was also reported in Refs. 14 & 29. For

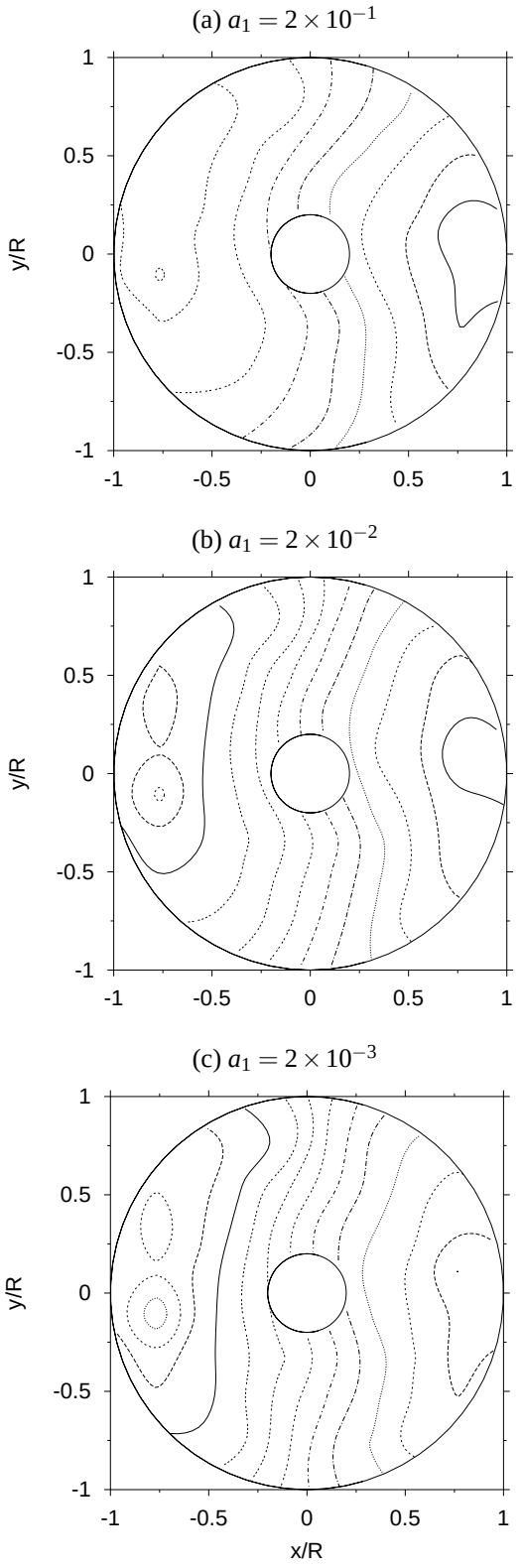

Figure 4: Contours of inflow in the rotor TPP using different values of the Squire's apparent or "eddy" viscosity parameter for the vortex core growth model. (a) $a_1 = 2 \times 10^{-1}$, (b) $a_1 = 2 \times 10^{-2}$, (c) $a_1 = 2 \times 10^{-3}$, and (d) $a_1 = 2 \times 10^{-4}$.

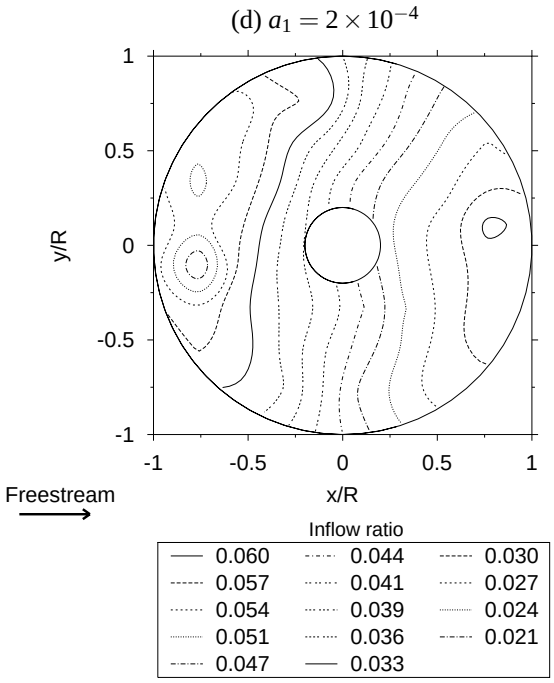

Figure 4: *Concluded.*

lower values of $a_1 = O\left(10^{-3}\right)$ and $O\left(10^{-4}\right)$ (less diffused vortices) these azimuthal variations are properly represented. This is especially apparent on the front of the rotor disk where the tip vortices remain close to the TPP. Therefore, on the basis of these numerical experiments it would appear that values of $a_1 = O\left(10^{-3}\right)$ to $O\left(10^{-4}\right)$ best describes the viscous core growth of rotor tip vortices. In the next section, available experimental evidence is examined to evaluate the validity of Squire's hypothesis, and to formalize an empirical value for the parameter, a_1.

Empirical Evidence of Turbulent Diffusion of Vorticity

The Lamb-Oseen core growth model given by Eq. 7 is valid for purely laminar flows, i.e., where viscous diffusion of vorticity takes place on the molecular level alone. In most practical cases of lift generated vortex flows, the vortex strengths and vortex Reynolds number are high enough to make it necessary to properly account for the effects of turbulent mixing on the development of the vortex core. Experimental measurements of vortex properties suggest that turbulent flow effects increase the rate of diffusion of vorticity from within the vortex core, similar to that expected based on Squire's hypothesis. These turbulent effects increase the mixing between layers of fluid inside the vortex, thereby enhancing the diffusion of vorticity in the radial direction.

The details of this process, however, are not clearly understood or documented, and experimental results have often been inconclusive. There is evidence that the inner core growth is dominated by viscous (laminar) effects, and the turbulent mixing effects there are small (Ref. 30). Other measurements suggest that there is turbulence generation at the edges of the laminar core (Ref. 31), which can influence net diffusive growth characteristics of the vortex. While the details still require further research, more readily derived vortex properties such as the peak swirl velocity and effective core size can be used to better understand the modeling requirements.

Following an approach similar to Iversen (Ref. 32), the present authors (Ref. 33) have shown a correlation between the non-dimensional peak swirl velocity and the age (or equivalent downstream distance) of the vortex. This correlation is of the form

$$\overline{V}_{\theta_{\max}} \left(\overline{d} + \overline{d}_0\right)^{\frac{1}{2}} = k \tag{14}$$

where the constants $\overline{d}_0$ and k were determined empirically. Such a correlation was found to be applicable to both fixed-wing and rotating-wing tip vortices, with several sets of experimental measurements coalescing to form a single universal curve – see Ref. 33 for details. The non-dimensional velocity, $\overline{V}_{\theta_{\max}}$, and non-dimensional downstream distance, $\overline{d}$, were defined as

$$\overline{V}_{\theta_{\max}} = \left(\frac{V_{\theta_{\max}}}{V_\infty}\right)\left(\frac{V_\infty c}{\Gamma_v}\right) \tag{15}$$

and

$$\overline{d} = \left(\frac{z}{c}\right)\left(\frac{\Gamma_v}{V_\infty c}\right) \tag{16}$$

respectively.

Examples of the correlation curves are shown for fixed-wing tip vortex measurements in Fig. 5(a), and for rotating-wings in Fig. 5(b). In both cases, the measurements show a definitive trend as given by Eq. 14. With the transformation $t = z/V_\infty$, the correlation given by Eq. 14 shows that

$$V_{\theta_{\max}} \propto \sqrt{\frac{\Gamma_v}{t}} \tag{17}$$

The maximum swirl velocity as given by the Lamb-Oseen (or Newman) model is

$$V_{\theta_{\max}} \propto \frac{\Gamma_v}{2\pi r_c} \propto \frac{\Gamma_v}{\sqrt{\delta \nu t}} \tag{18}$$

Therefore,

$$V_{\theta_{\max}} \propto \sqrt{\frac{\Gamma_v}{t}} \sqrt{\frac{1}{\delta}\left(\frac{\Gamma_v}{\nu}\right)} \tag{19}$$

Comparing Eqs. 17 & 19, it follows that

$$\frac{1}{\delta}\left(\frac{\Gamma_v}{\nu}\right) = \frac{Re_v}{\delta} = \text{constant} \tag{20}$$

(a) Fixed-wing tip vortex measurements from Ref. 2.

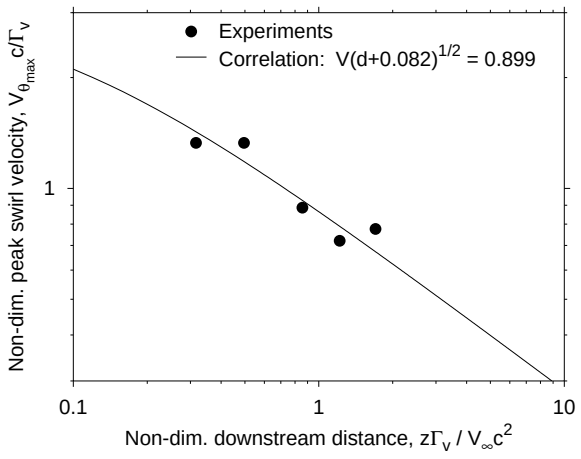

(b) Rotor tip vortex measurements from Ref. 25.

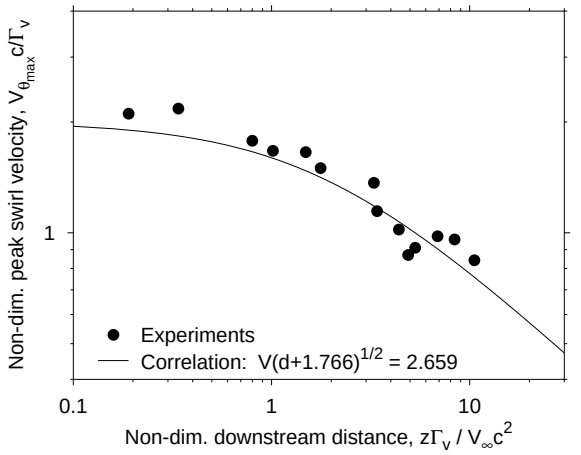

Figure 5: Correlation of peak swirl velocity as a function of downstream distance from the vortex origin as given by Eq. 14. (a) Fixed-wing tip vortex measurements from Ref. 2. (b) Rotor tip vortex measurements from Ref. 25.

which means that the average apparent viscosity coefficient, δ, is proportional to the vortex Reynolds number, Re_v. Therefore, the correlations previously reported by Iversen (Ref. 32) and by Bhagwat & Leishman (Ref. 33) support Squire's hypothesis, which relates the average apparent viscosity coefficient to the vortex Reynolds number, as given by Eq. 13. Therefore, vortex diffusion effects will be expected to increase with increasing vortex Reynolds number, Re_v.

A recent study of fixed-wing trailing vortices reported by Cotel & Breidenthal (Ref. 34) suggests that the diffusion of vorticity in the vortex is dominated by laminar flow effects. These authors conclude based on the ideas of flow stratification in the vortex core, that the effects of turbulence on vortex core growth are almost negligi-

ble, with the vortex flow being governed by laminar diffusion alone. The attainment of a critical Richardson's number essentially suggests that the strong rotational velocity in the vortex core causes the re-laminarization of any turbulence formed inside the core or which may be entrained from outside the vortex core. This results in a predominantly laminar vortex core development. Similar observations have been reported for rotating wing measurements (Ref. 30), where the vortex core initially grows very slowly, almost laminar-like. This is followed by a more rapid but asymptotic growth in the core as the tip vortex structure becomes more turbulent as it mixes with the inner vortex sheet.

Cotel & Breidenthal (Ref. 34) present results from several trailing vortex measurements in the form of a non-dimensional core growth rate, b_1, as defined by

$$b_1 = 2\sqrt{\frac{t}{\Gamma_v}}\left(\frac{dr_c}{dt}\right) \tag{21}$$

The growth rate is shown to be inversely proportional to the square root of the vortex Reynolds number, suggesting purely laminar viscous diffusion. This trend was deduced in the analysis of several experimental measurements reported in Ref. 34. Indeed, using the Lamb-Oseen core growth model as given by Eq. 7 it follows from Eq. 21 that

$$b_1 \propto Re_v^{-\frac{1}{2}} \tag{22}$$

The extended core growth model of Eq. 11 would show this trend for the case where the apparent viscosity ratio, δ, is a constant independent of the vortex Reynolds number. Recall that $\delta = 1$ corresponds to the laminar case, and a constant value of δ would also suggest that the core growth is essentially laminar. However, the experimental data reported in Ref. 34 was from small-scale tests and was restricted to vortex Reynolds numbers smaller than 10^5.

Iversen (Ref. 32) reports that the turbulent flow effects in the vortex core become important only for vortex Reynolds numbers greater than 10^5. The flow stratification argument presented in Ref. 34 explains how externally entrained turbulence, such as from a vortex sheet, would not influence the predominantly laminar core growth. However turbulence generation within the vortex core (e.g., see Ref. 31) may affect its diffusive growth. Indeed, using the core growth model in Eq. 11 the core growth rate can be shown to be proportional to

$$b_1 \propto \sqrt{\delta}\, Re_v^{-\frac{1}{2}} \tag{23}$$

and using the definition of δ as given by Squire's hypothesis (Eq. 13), it can be shown that

$$b_1 \propto \sqrt{a_1} + Re_v^{-\frac{1}{2}} \tag{24}$$

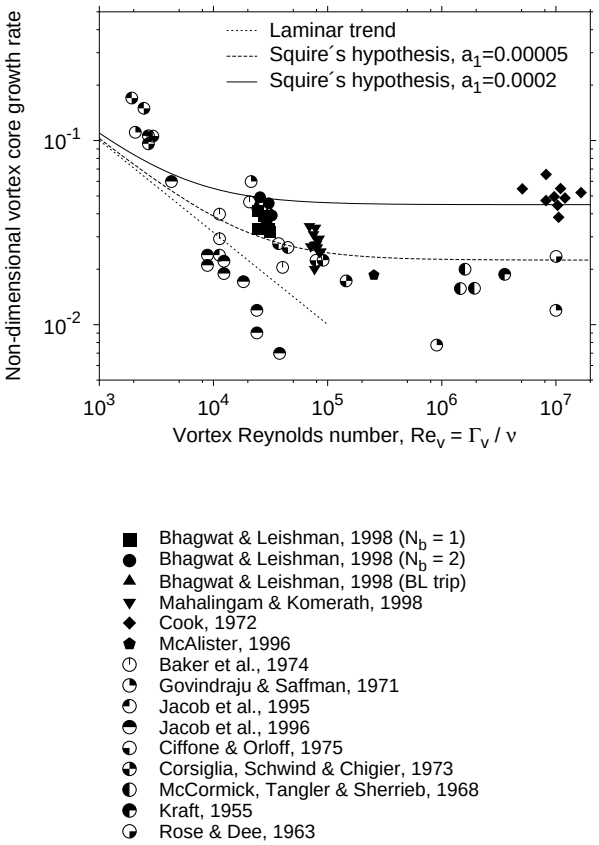

Figure 6: Non-dimensional viscous core growth rate for several trailing vortex measurements as a function of vortex Reynolds number.

Therefore, a predominantly laminar core growth trend may be observed for smaller values of vortex Reynolds numbers, typically found in small-scale experiments. However, for large values of vortex Reynolds numbers the core growth rate would become asymptotically constant, as governed by the constant value of the Squire's parameter, a_1.

Figure 6 shows the results reported in Ref. 34 along with an assemblage of additional data from several other sources of experimental tip vortex measurements (Refs. 25, 35–46), which include full-scale fixed-wing as well as rotating-wing trailing vortices. Lines are shown for the predominantly laminar trend, as in Ref. 34, along with the trends obtained on the basis of Squire's hypothesis.

For smaller Reynolds numbers, the experiments show a somewhat laminar-like trend for the growth of the vortices. Yet, at larger Reynolds numbers, the core growth rate appears to remain nominally constant. The trend lines for Squire's hypothesis suggest that this behavior is be-

(a) Apparent viscosity coefficient, δ.

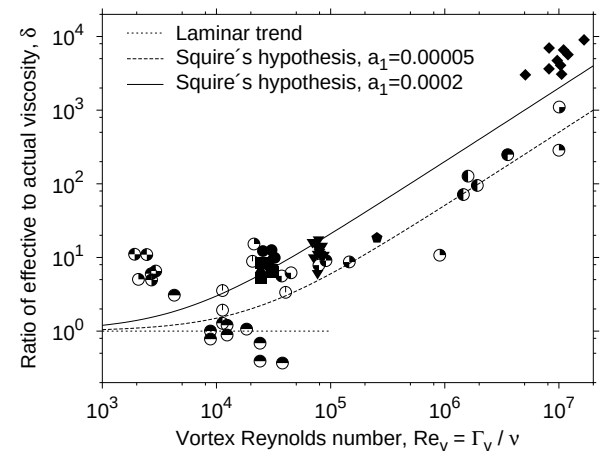

(b) Squire's apparent viscosity parameter a_1.

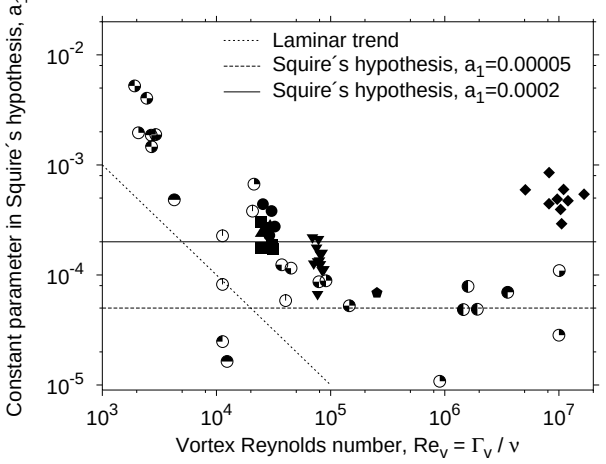

Figure 7: Apparent or average "eddy" viscosity in the vortex core growth as a function of vortex Reynolds number. (a) Apparent or "eddy" viscosity coefficient, δ. (b) Squire's apparent viscosity parameter a_1 (Ref. 3). See Fig. 6 for legend describing experimental results.

cause of turbulent diffusion of vorticity from within the vortex. Notice that the trend given by Squire's hypothesis also describes the vortex core growth as essentially laminar at low vortex Reynolds numbers, with turbulent diffusion effects becoming apparent only at the higher Reynolds numbers.

The same results are presented again in Fig. 7(a) as an average apparent viscosity coefficient, δ as a function of vortex Reynolds number. For low Reynolds numbers, the measurements indicate a nominally constant values of δ, suggesting that the core is mostly laminar. However, the turbulence effects are manifest as increasing average apparent viscosity with increasing Reynolds number, with an almost linearly increasing trend at high Reynolds numbers. Notice that experimental values of $\delta < 1$ imply that turbulent mixing results in an even smaller amount of vorticity diffusion than the laminar case, which is physically impossible. However, the various uncertainties in experimental measurements may account for such inconsistencies, and highlights the difficulties in making such measurements on vortices. The overall experimental evidence, however, strongly suggests the validity of Squire's hypothesis that turbulent diffusion of vorticity from within the vortex core is directly proportional to the vortex Reynolds number, as given by Eq. 13.

The results are shown in Fig. 7(b) in the form of the Squire's parameter, a_1. The assemblage of experimental data suggests that the apparent viscosity parameter falls in the range $O\left(10^{-3}\right)$ to $O\left(10^{-4}\right)$, as was also deduced from the free-vortex wake predictions presented earlier. It appears that the rotating-wing results show a slightly higher viscous diffusion rate corresponding to an average value of $a_1 = O\left(10^{-4}\right)$, while the fixed-wing results show a lower net diffusion rate with $a_1 = O\left(10^{-5}\right)$.

It must be recognized, however, that most rotating-wing results have the implicit effects of vortex straining resulting from filament curvature and other wake distortion effects included in the measurements, which may account for part of these differences. Isolating the viscous effects associated with diffusion of vorticity from those associated with strain or vortex stretching will be a problem for future consideration (Ref. 47). Clearly, however, the average value of a_1 is of the order of 10^{-3} to 10^{-5} for all the data shown here.

Therefore, on the basis of the foregoing results, Eq. 11 provides a preliminary universal model for the growth of the viscous core of a trailing tip vortex, with the value of the empirical parameter a_1 being determined from experiments as described above. The initial core radius of trailing vortices has been measured to be typically $5-10\%$ of chord, i.e., of the order of the airfoil thickness at the wing tip where the vortex was originated. The effective origin offset, z_0 or ζ_0, can then be established from the initial core radius, r_{c_0}, by using Eqs. 11 or 12.

Solution for Self-Similar Vortex Velocity Profiles

The tip vortex flow can now be examined in a cylindrical coordinate system with the origin at the blade tip where the vortex first originated. The vortex trajectory, which is along the longitudinal axis of the vortex (z-axis), is fixed relative to the wing or blade tip, i.e., the vortex is examined under steady flow conditions. It should be noted that the axial velocity relative to the wing is the sum of the free-stream velocity and the vortex induced velocity, i.e., $V_\infty + V_z$.

The induced velocities are assumed to be dependent only on r and z, i.e., the vortex is assumed to be axisymmetric. This is a reasonable assumption because even though, in practice, both fixed and rotating wing tip vortices are not completely axisymmetric, the asymmetry is usually small and restricted to small regions close to the origin of the vortex.* As the vortex convects downstream, the velocity profiles become more axisymmetric.

The governing Navier-Stokes equations for incompressible flow as written in cylindrical coordinates are:

Continuity

$$\frac{1}{r}\frac{\partial}{\partial r}(rV_r)+\frac{\partial V_z}{\partial z}=0 \tag{25}$$

$r-momentum$

$$V_r\frac{\partial V_r}{\partial r}+V_\infty\frac{\partial V_r}{\partial z}+V_z\frac{\partial V_r}{\partial z}-\frac{V_\theta^2}{r} = -\frac{1}{\rho}\frac{\partial p}{\partial r}+\nu\left[\nabla^2 V_r-\frac{V_r}{r^2}\right] \tag{26}$$

$\theta-momentum$

$$V_r\frac{\partial V_\theta}{\partial r}+V_\infty\frac{\partial V_\theta}{\partial z}+V_z\frac{\partial V_\theta}{\partial z}+\frac{V_rV_\theta}{r} = \nu\left[\nabla^2 V_\theta-\frac{V_\theta}{r^2}\right] \tag{27}$$

$z-momentum$

$$V_r\frac{\partial V_z}{\partial r}+V_\infty\frac{\partial V_z}{\partial z}+V_z\frac{\partial V_z}{\partial z}=-\frac{1}{\rho}\frac{\partial p}{\partial z}+\nu\left[\nabla^2 V_z\right] \tag{28}$$

where the operator ∇^2 is given by

$$\nabla^2=\frac{\partial^2}{\partial r^2}+\frac{1}{r}\frac{\partial}{\partial r}+\frac{\partial^2}{\partial z^2} \tag{29}$$

The required boundary conditions can be obtained by assuming that the vortex is generated as a "free" vortex, i.e., a potential vortex of strength Γ_v at $z=0$, and it diffuses until at large distances the vortex induced velocities become zero – see Ref. 17. These boundary conditions can be formalized as:

1. At $z=0$, $V_\theta=\Gamma_v/2\pi r$ and $V_z,V_r=0$. Notice that there is a singularity at $r=0$.
2. For $z>0$, $V_\theta,V_z,V_r\longrightarrow 0$ for large r.
3. As $z\longrightarrow\infty$, $V_\theta,V_z,V_r\longrightarrow 0$ for all r.

*Flow measurements made with the convecting vortices generated by rotating wings must be placed in axis system moving with the vortex core using either a Galilean or Reynolds type decomposition of the flow – see Ref. 30.

The governing Navier-Stokes equations are now rewritten in a non-dimensional form so as to allow some simplifications. The velocities are normalized with the free-stream velocity, V_∞, i.e.,

$$\overline{V_i}=\frac{V_i}{V_\infty},\quad i=r,\theta,z \tag{30}$$

The distances are normalized by the wing chord length, c, i.e.,

$$\overline{r}=\frac{r}{c}\quad\text{and}\quad\overline{z}=\frac{z}{c} \tag{31}$$

The pressure is normalized with the dynamic pressure

$$\overline{p}=\frac{p}{\rho V_\infty^2} \tag{32}$$

and the flow Reynolds number is given by

$$Re=\frac{V_\infty\, c}{\nu} \tag{33}$$

To simplify the governing equations, an ordering scheme may be employed to establish the relative magnitudes of the non-dimensional terms. The swirl and axial velocities induced by the tip vortex are small as compared to the free-stream velocity, typical values being 0.1 to 0.3 (see Refs. 2, 25, 35, 48–50), i.e., $\overline{V_\theta}$ and $\overline{V_z}$ are $O(\varepsilon)$. Typically the tip vortex core radius is of the order of the airfoil thickness (e.g., Refs. 24, 51), which is typically 5 to 15% of the wing or blade chord. The tip vortex can be observed, and induces significant velocities, for several chord lengths downstream of the generating wing. This implies that, if $\overline{z}$ is $O(1)$ then $\overline{r}$ is $O(\varepsilon)$.

The continuity equation now implies that the radial velocity, $\overline{V_r}$, is $O(\varepsilon^2)$. This is also consistent with the observation that the radial velocities induced by the tip vortices are very small (Ref. 2). The radial momentum equation (Eq. 26) indicates that the pressure, $\overline{p}$, is $O(\varepsilon^2)$. Typically, for a transport aircraft or a helicopter rotor, the chord Reynolds number is approximately 10^7. Even in wind tunnel experiments with scaled models, the Reynolds numbers are always greater than 10^4. Therefore, Re can be assumed to be $O(1/\varepsilon^4)$.

The conservation laws are now rewritten in the non-dimensional form with the order of magnitudes of each term being indicated below each term. Notice that, all the variables are non-dimensional, but the overbar has been omitted.

Continuity :

$$\underset{\varepsilon}{\frac{1}{r}\frac{\partial}{\partial r}(rV_r)}\quad+\quad\underset{\varepsilon}{\frac{\partial V_z}{\partial z}}\quad=\quad 0 \tag{34}$$

$r-momentum$:

$$\begin{array}{ccccccc} V_r\dfrac{\partial V_r}{\partial r} & + & \dfrac{\partial V_r}{\partial z} & + & V_z\dfrac{\partial V_r}{\partial z} & - & \dfrac{V_\theta^2}{r} \\ \varepsilon^3 & & \varepsilon^2 & & \varepsilon^3 & & \varepsilon \end{array} =$$

$$\begin{array}{ccc} -\dfrac{\partial p}{\partial r} & + & \dfrac{1}{Re}\left[\nabla^2 V_r - \dfrac{V_r}{r^2}\right] \\ \varepsilon & & \varepsilon^4 \end{array} \tag{35}$$

$\theta-momentum$:

$$\begin{array}{ccccccc} V_r\dfrac{\partial V_\theta}{\partial r} & + & \dfrac{\partial V_\theta}{\partial z} & + & V_z\dfrac{\partial V_\theta}{\partial z} & + & \dfrac{V_r V_\theta}{r} \\ \varepsilon^2 & & \varepsilon & & \varepsilon^2 & & \varepsilon^2 \end{array} =$$

$$\begin{array}{c} \dfrac{1}{Re}\left[\nabla^2 V_\theta - \dfrac{V_\theta}{r^2}\right] \\ \varepsilon^3 \end{array} \tag{36}$$

$z-momentum$:

$$\begin{array}{ccccccc} V_r\dfrac{\partial V_z}{\partial r} & + & \dfrac{\partial V_z}{\partial z} & + & V_z\dfrac{\partial V_z}{\partial z} \\ \varepsilon^2 & & \varepsilon & & \varepsilon^2 \end{array} =$$

$$\begin{array}{ccc} -\dfrac{\partial p}{\partial z} & + & \dfrac{1}{Re}\left[\nabla^2 V_z\right] \\ \varepsilon^2 & & \varepsilon^3 \end{array} \tag{37}$$

One approach to simplify these governing equations (Eqs. 34–37) is to linearize them by neglecting the higher order terms in ε. This results in the simplified set of equations:

$$\begin{aligned} \frac{1}{r}\frac{\partial}{\partial r}(rV_r) + \frac{\partial V_z}{\partial z} &= 0 \\ \frac{\partial p}{\partial r} - \frac{V_\theta^2}{r} &= 0 \\ \frac{\partial V_\theta}{\partial z} &= 0 \\ \frac{\partial V_z}{\partial z} &= 0 \end{aligned} \tag{38}$$

Clearly, these equations alone are not sufficient to solve for the vortex induced velocity profiles. Therefore, a different approach must be employed to further simplify the governing equations.

The proposed simplification approach proceeds with a pre-assumed solution for the swirl velocity in the tip vortex. The swirl velocity is chosen to be the algebraic profile first suggested by Vatistas (Ref. 21), as given by the expression

$$V_\theta(r) = \frac{\Gamma_v}{2\pi}\left\{\frac{r}{\left(r_c^{2n}+r^{2n}\right)^{1/n}}\right\} \tag{39}$$

or

$$V_\theta(\bar{r}) = \frac{\Gamma_v}{2\pi r_c}\left\{\frac{\bar{r}}{\left(\bar{r}^{2n}+1\right)^{1/n}}\right\} \tag{40}$$

with the exponent n taking only integer values. Notice that r_c is the viscous core radius of the tip vortex, that is the swirl velocity exhibits a maximum at $r = r_c$. As previously mentioned, this algebraic velocity profile has shown to give good agreement with experimental measurements, and is an approximation to the Lamb-Oseen solution (Eq. 8), i.e., an approximate solution to the one-dimensional Navier-Stokes equation

$$V_\infty\frac{\partial V_\theta}{\partial z} = \nu\left[\nabla^2 V_\theta - \frac{V_\theta}{r^2}\right] \tag{41}$$

The θ-momentum equation can now be simplified by subtracting the one-dimensional form (Eq. 41) from Eq. 36 resulting in

$$V_r\frac{\partial V_\theta}{\partial r} + V_z\frac{\partial V_\theta}{\partial z} + \frac{V_r V_\theta}{r} = 0 \tag{42}$$

This forms the third equation along with the first two equations in Eq. 38 to give a simplified set of governing equations

$$\left.\begin{aligned} \frac{1}{r}\frac{\partial}{\partial r}(rV_r) + \frac{\partial V_z}{\partial z} &= 0 \\ V_r\frac{\partial V_\theta}{\partial r} + V_z\frac{\partial V_\theta}{\partial z} + \frac{V_r V_\theta}{r} &= 0 \\ \frac{\partial p}{\partial r} - \frac{V_\theta^2}{r} &= 0 \end{aligned}\right\} \tag{43}$$

Therefore, with the swirl velocity profile being given by Eq. 39, the pressure and the radial and axial induced velocity profiles can be determined as solution to the above set of equations. The axial and radial velocity components are solved for by satisfying first two equations, i.e., the continuity equation (Eq. 25) and Eq. 42. These components are given by

$$V_z = -\frac{A}{z}\left\{1 - \frac{r^2}{\left(r_c^{2n}+r^{2n}\right)^{1/n}}\right\} \tag{44}$$

$$V_r = -\frac{Ar}{2z^2}\left\{1 - \frac{r^2}{\left(r_c^{2n}+r^{2n}\right)^{1/n}}\right\} \tag{45}$$

where A is a constant. Notice that depending on the sign of A, the axial velocity can be either "wake-like" or "jet-like."

(a) Swirl (tangential) velocity.

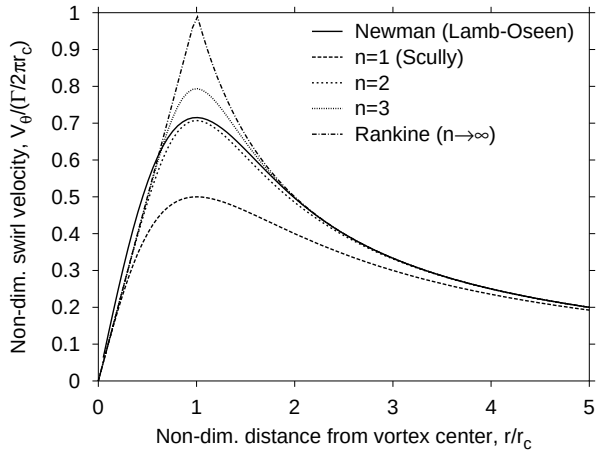

(b) Radial velocity.

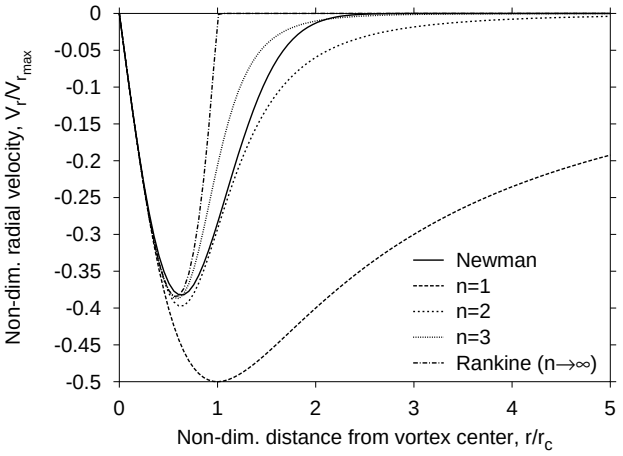

(c) Axial velocity.

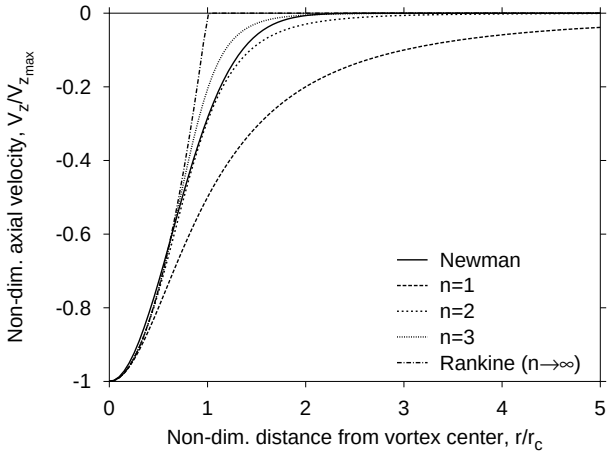

Figure 8: Vortex induced velocities given by the present model for various values of the parameter n. The Newman model (Ref. 17) is also shown for comparison. (a) Swirl (tangential) velocity. (b) Radial velocity. (c) Axial velocity. (d) Static pressure distribution in the vortex core.

(d) Static pressure distribution

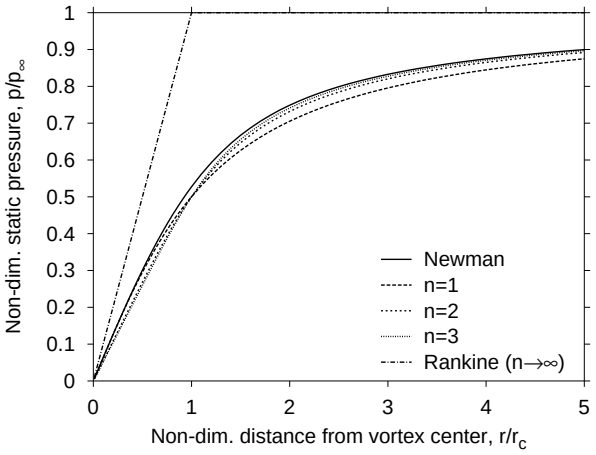

Figure 8: *Concluded.*

Following the approach taken by Newman (Ref. 17), the constant A may be determined based on the drag of the generating wing as given by

$$A = \frac{D_0}{4\pi\rho\,(\delta\nu)} \tag{46}$$

where the drag, D_0, on the wing in the limit as $\Gamma \to 0$ can be expressed in terms of the zero-lift drag coefficient of the airfoil section, C_{d_0}, as

$$D_0 = \frac{1}{2}\rho V_\infty^2 c \left(\frac{b}{2}\right) C_{d_0} \tag{47}$$

where $b/2$ is the wing semi-span. For the rotating wing case, the average profile drag, D_0, on the blade is given by integration of the sectional drag to get

$$D_0 = \frac{1}{2}\rho\,(\Omega R)^2\, c \left(\frac{R}{3}\right) C_{d_0} \tag{48}$$

where Ω is the rotational speed, and R the radius of the rotor. If the profile power of the rotor, P_0, is known or measured (say by extrapolating the power versus thrust curve to zero thrust), then D_0 is related to P_0 using

$$D_0 = \frac{4}{3}\left(\frac{P_0}{N_b \Omega R}\right) \tag{49}$$

where N_b is the number of blades.

The static pressure distribution in the vortex can be determined by integrating third part of Eq. 43 with respect to r, i.e.,

$$p(r) = \int_0^r \frac{V_\theta^2}{r} dr \tag{50}$$

The non-dimensional induced velocity profiles given by this model for different values of the parameter n are shown in Fig. 8. As the parameter $n \to \infty$, the present

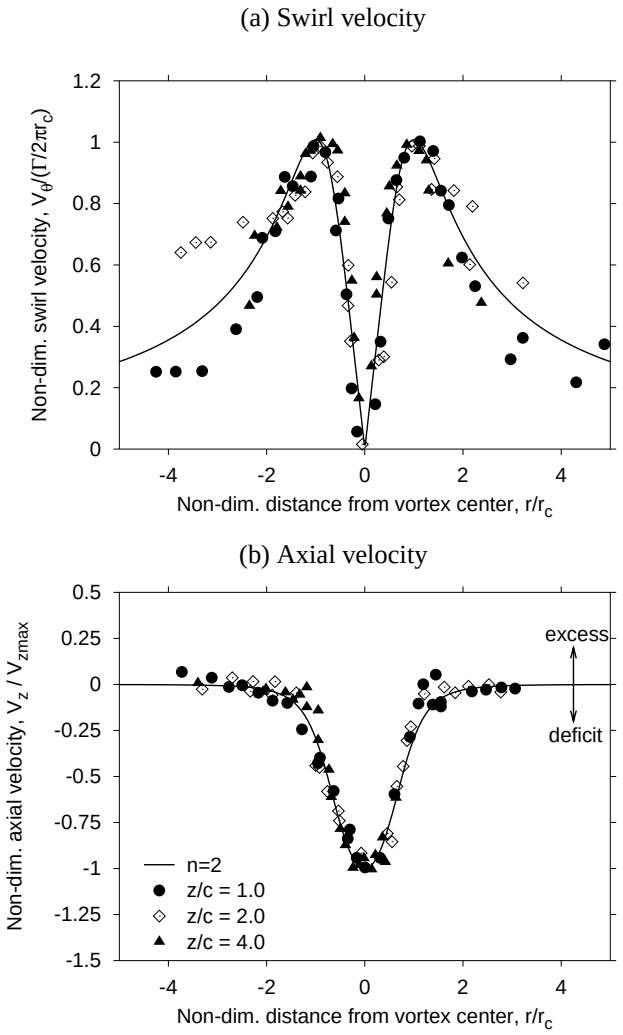

Figure 9: Comparison of vortex induced velocities using the proposed model $(n = 2)$ with fixed-wing experimental results (Ref. 2). (a) Swirl velocity. (b) Axial velocity.

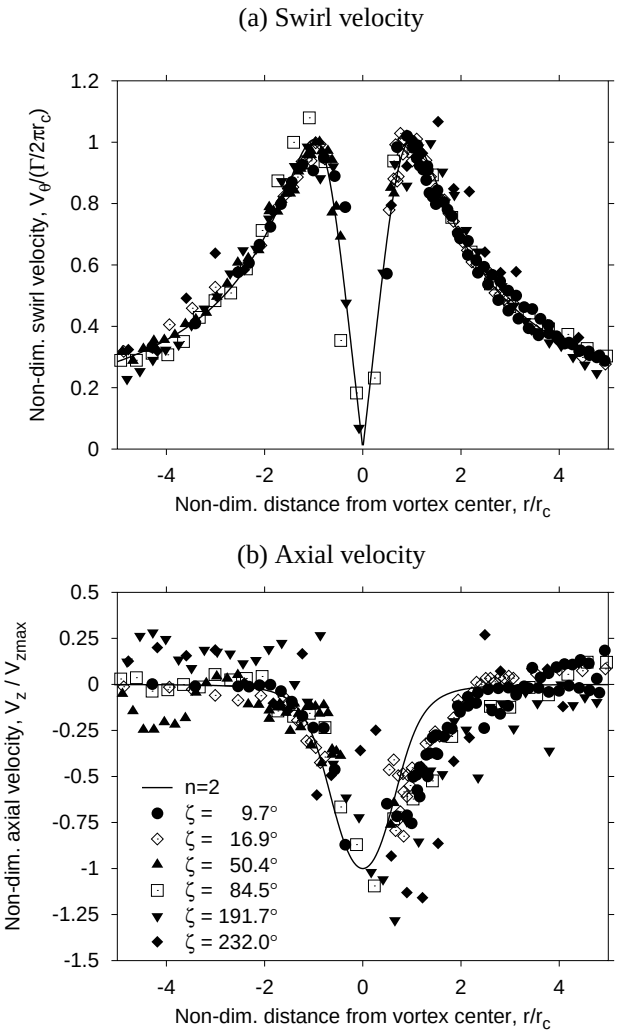

Figure 10: Comparison of vortex velocities using the proposed model $(n = 2)$ with rotating-wing experimental results (Ref. 25). (a) Swirl velocity. (b) Axial velocity.

model reduces to the Rankine vortex model with a solid body rotation of the vortex core. The exponential velocity model proposed by Newman (Ref. 17) is also shown for comparison. Recall that for the swirl velocity the Newman model is identical to the Lamb-Oseen model. For the value of $n = 2$, the present model closely resembles the Newman model, thus verifying that it is, indeed, an algebraic approximation to a solution of the Navier-Stokes solution.

The results obtained using the proposed algebraic vortex model are now compared with experimentally measured vortex induced velocities for both fixed-wing and rotating-wing tip vortices. Figure 9 shows the swirl and axial velocities in the tip vortex generated by a fixed wing, with the experimental results from Dosanjh et al. (Ref. 2). Both velocity profiles are non-dimensionalized with the maximum velocity in the viscous vortex core, while the radial distance is normalized with the vortex core radius, as defined previously. Both the measured velocity profiles are found to be essentially self-similar, and the present model showed good agreement with experiments when using the parameter $n = 2$.

Figure 10 shows results for a rotating-wing tip vortex, with the experimental data taken from Ref. 25. In this case, the measured swirl velocity data showed a strongly self-similar profile, and the present model showed close agreement with this observed trend. The axial velocity measurements showed some asymmetric deviations from the self-similar profile. However, overall agreement with the present model for the $n = 2$ case is considered good.

The radial velocities in the tip vortex are noted to be of much smaller magnitude, as described previously. There-

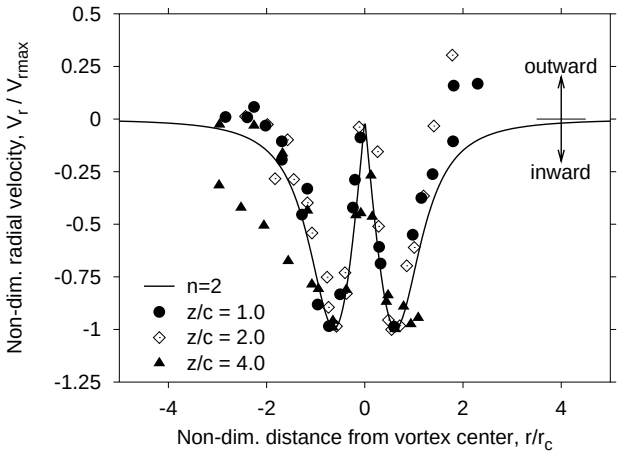

Figure 11: Radial velocity profiles in the trailing vortex of a fixed wing tip vortex compared with the present model. Experimental measurements from Ref. 2.

fore, the radial velocities are more sensitive to measurement uncertainties, and accurate measurements of radial velocity are, in general, more difficult for rotating-wing tip vortices, e.g., see Ref. 30. The measured velocity distribution from Ref. 2 is shown in Fig. 11. The results showed some scatter resulting from uncertainties in the measurements, but the overall trend agrees with that predicted using the present model for $n = 2$.

Conclusions

The diffusive growth of a viscous vortex has been modeled using an extension of the classic Lamb-Oseen core growth model with an average apparent or eddy viscosity correction for the effects of self-generated turbulence. The apparent viscosity parameter, as given by Squire's hypothesis, was estimated based on several sets of experimental results documenting the characteristics of trailing tip vortices. A family of algebraic models for the three components of velocity induced by a viscous trailing tip vortex has been proposed. The velocity components were determined by solving a simplified form of the incompressible Navier-Stokes equations. The model has been compared with velocity field measurements for both fixed-wing and rotating-wing tip vortices.

The observations and conclusions from this study are summarized as follows:

1. The classic Lamb-Oseen model for the viscous core growth of a vortex accounts only for laminar diffusion of vorticity. Squire's hypothesis suggests a correction to this basic laminar model using an average apparent viscosity parameter. Available experimental measurements were examined to show the validity of Squire's hypothesis in that the diffusion of vorticity is governed by an apparent turbulent viscosity that is proportional to the vortex Reynolds number. A general empirical value for the apparent viscosity parameter has been suggested.

2. In the proposed vortex model, the three components of the vortex induced velocity are continuous, bounded, and asymptote to zero at large distances. The swirl velocity shows a behavior similar to the one-dimensional Lamb-Oseen vortex. The axial velocity in the vortex core shows a wake-like profile, with the maximum velocity deficit occurring at the center of the vortex. The radial velocity induced by the tip vortex is directed toward the vortex center, with a maximum value occurring inside the vortex core radius. The magnitude of the radial velocity was found to be much smaller than the swirl or the axial velocities.

3. Free-vortex wake predictions were shown to be sensitive to the assumption made for the vortex core growth model. By choosing the core growth parameters as outlined in this study, the free-vortex wake predictions gave improved agreement with measured wake geometries, as well as provided better predictions of the higher harmonic variations of the rotor inflow.

4. The proposed model provides solutions for the vortex induced profiles in the form of a family of algebraic profiles with an integer parameter n. For the case of $n = 2$, the proposed model was shown to give good predictions of the characteristics of both fixed-wing and rotating-wing tip vortices. Therefore, this general model should be suitable for use in several aeroacoustic applications that require good physical approximations for the viscous nature of tip vortices.

Acknowledgments

This work was partly supported by the National Rotorcraft Technology Center under Grant NCC 2944. Drs. Thomas Doligalski and Yung Yu were the technical monitors.

References

[1]Various Authors, Conference on Capacity and Wake Vortices, Imperial College of Science, Technology & Medicine, London, UK, September 11–14, 2001.

[2]Dosanjh, D. S., Gasparek, E. P., and Eskinazi, S., "Decay of a Viscous Trailing Vortex," *The Aeronautical Quarterly*, Vol. 3, No. 3, 1962, pp. 167–188.

[3]Squire, H. B., "The Growth of a Vortex In Turbulent Flow," *Aeronautical Quarterly*, Vol. 16, August 1965, pp. 302–306.

[4]Owen, P. R., "The Decay of a Turbulent Trailing Vortex," *The Aeronautical Quarterly*, Vol. 10, February 1969, pp. 69–78.

[5]Widnall, S. E., "The Structure and Dynamics of Vortex Filaments," *Annual Review of Fluid Mechanics*, Vol. 7, 1975, pp. 141–165.

[6]Sarpkaya, T., "Decay of Wake Vortices of Large Aircraft," *AIAA Journal*, Vol. 36, No. 9, September 1998, pp. 1671–1679.

[7]Kantha, L. H., "Empirical Model of Transport and Decay of Aircraft Wake Vortices," *Journal of Aircraft*, Vol. 35, No. 4, April 1998, pp. 649–652.

[8]Spalart, P. R., "Airplane Trailing Vortices," *Annual Review of Fluid Mechanics*, Vol. 30, 1998, pp. 107–138.

[9]McCroskey, W. J., "Vortex Wakes of Rotorcraft," AIAA Paper 95-0530, 33^{rd} AIAA Aerospace Sciences Meeting and Exhibit, Reno, NV, January 9–12, 1995.

[10]Leishman, J. G., and Bagai, A., "Challenges in Understanding the Vortex Dynamics of Helicopter Rotor Wakes," *AIAA Journal*, Vol. 36, No. 7, July 1998, pp. 1130–1140.

[11]Johnson, W., "Wake Model for Helicopter Rotors in High Speed Flight," NASA CR-1177507, USAVSCOM TR-88-A-008, November 1988.

[12]Bagai, A., and Leishman, J. G., "Rotor Free-Wake Modeling Using a Relaxation Technique - Including Comparisons with Experimental Data," *Journal of the American Helicopter Society*, Vol. 40, No. 3, July 1995, pp. 29–41.

[13]Bhagwat, M. J., and Leishman, J. G., "Stability, Consistency and Convergence of Time-Marching Free-Vortex Rotor Wake Algorithms," *Journal of the American Helicopter Society*, Vol. 46, No. 1, January 2001, pp. 59–71.

[14]Gandhi, F., and Tauszig, L., "A Critical Evaluation of Various Approaches for the Numerical Detection of Helicopter Blade-Vortex Interactions," *Journal of the American Helicopter Society*, Vol. 45, No. 3, 2000, pp. 179–190.

[15]Lamb, H., *Hydrodynamics*, 6^{th} ed., Cambridge University Press, Cambridge, UK, 1932.

[16]Burgers, J. M., "A Mathematical Model Illustrating the Theory of Turbulence," *Advances in Applied Mechanics*, Vol. 1, 1948, pp. 171–199.

[17]Newman, B. G., "Flow in a Viscous Trailing Vortex," *The Aeronautical Quarterly*, Vol. 1, May 1959, pp. 167–188.

[18]Ogawa, A., *Vortex Flow, CRC Series on Fine Particle Science and Technology* CRC Press Inc., 1993.

[19]Scully, M. P., and Sullivan, J. P., "Helicopter Rotor Wake Geometry and Airloads and Development of Laser Doppler Velocimeter for Use in Helicopter Rotor Wakes," Massachusetts Institute of Technology Aerophysics Laboratory Technical Report 183, MIT DSR No. 73032, August 1972.

[20]Kaufmann, W., "Uber die Ausbreitung kreiszlindrischer Wirbel in zahen Flussigkeiten," *Ing. Arch.*, Vol. 31, No. 1, 1962, p. 1.

[21]Vatistas, G. H., Kozel, V., and Mih, W. C., "A Simpler Model for Concentrated Vortices," *Experiments in Fluids*, Vol. 11, 1991, pp. 73–76.

[22]Vatistas, G. H., "New Model for Intense Self-Similar Vortices," *Journal of Propulsion and Power*, Vol. 14, No. 4, April 1998, pp. 462–469.

[23]Coyne, A. J., Bhagwat, M. J., and Leishman, J. G., "Investigation into the Rollup and Diffusion of Rotor Tip Vortices using Laser Doppler Velocimetry," American Helicopter Society 53^{rd} Annual National Forum, Virginia Beach, VA, April 29–May 1, 1997.

[24]Bagai, A., and Leishman, J. G., "Flow Visualization of Compressible Vortex Structures Using Density Gradient Techniques," *Experiments in Fluids*, Vol. 15, 1993, pp. 431–442.

[25]Bhagwat, M. J., and Leishman, J. G., "Measurements of Bound and Wake Circulation on a Helicopter Rotor," *Journal of Aircraft*, Vol. 37, No. 2, March-April 2000, pp. 227–234.

[26]Rankine, W. J. M., *Manual of Applied Mechanics*, C. Griffen Co., London, 1858.

[27]Scully, M. P., "Computation of Helicopter Rotor Wake Geometry and Its Influence on Rotor Harmonic Airloads," Massachusetts Institute of Technology Report No. ASRL TR 178-1, March 1975.

[28]Oseen, C. W., "Uber Wirbelbewegung in Einer Reibenden Flussigkeit," *Ark. J. Mat. Astrom. Fys.*, Vol. 7, 1912, pp. 14–21.

[29]Lim, J., and Tung, C., "2GCHAS Predictions of HART Blade-Vortex Interaction Loading," Proceedings of the AHS Technical Specialists' Meeting for Rotorcraft Acoustics and Aerodynamics, Williamsburg, VA, October 28–30, 1997.

[30]Martin, P. B., Pugliese, G., and Leishman, J. G., "High Resolution Trailing Vortex Measurements in the Wake of a Hovering Rotor," American Helicopter Society 57th Annual National Forum, Washington, DC, May 9–11, 2001.

[31]Han, Y. O., Leishman, J. G., and Coyne, A. J., "On the Turbulent Structure of a Tip Vortex Generated by a Rotor," *AIAA Journal*, Vol. 35, No. 3, March 1997, pp. 477–485.

[32]Iversen, J. D., "Correlation of Turbulent Trailing Vortex Decay Data," *Journal of Aircraft*, Vol. 13, No. 5, May 1976, pp. 338–342.

[33]Bhagwat, M. J., and Leishman, J. G., "Correlation of Helicopter Tip Vortex Measurements," *AIAA Journal*, Vol. 38, No. 2, February 2000, pp. 301–308.

[34]Cotel, A. J., and Breidenthal, R. E., "Turbulence Inside a Vortex," *Physics of Fluids*, Vol. 11, No. 10, October 1999, pp. 3026–3029.

[35]Mahalingam, R., and Komerath, N. M., "Measurements of the Near Wake of a Rotor in Forward Flight," AIAA Paper 98-0692, 36th Aerospace Sciences Meeting & Exhibit, Reno, NV, January 12–15, 1998.

[36]Cook, C. V., "The Structure of the Rotor Blade Tip Vortex," Paper 3, Aerodynamics of Rotary Wings, AGARD CP-111, September 13–15, 1972.

[37]McAlister, K. W., "Measurements in the Near Wake of a Hovering Rotor," AIAA Paper 96-1958, 27th AIAA Fluid Dynamic Conference, New Orleans, June 18–20, 1996.

[38]Baker, G. R., Barker, S. J., Bofah, K. K., and Saffman, P. G., "Laser Anemometer Measurements of Trailing Vortices in Water," *Journal of Fluid Mechanics*, Vol. 65, 1974, pp. 325–336.

[39]Govindraju, S. P., and Saffman, P. G., "Flow in a Turbulent Trailing Vortex," *Physics of Fluids*, Vol. 14, No. 10, October 1971, pp. 2074–2080.

[40]Jacob, J., Savas, O., and Liepmann, D., "Trailing Vortex Wake Growth Characteristics of a High Aspect Ratio Rectangular Airfoil," *AIAA Journal*, Vol. 35, 1995, p. 275.

[41]Jacob, J., Savas, O., and Liepmann, D., "Experimental Investigation of Forced Wake Vortices on a Rectangular Wing," AIAA Paper 96-2497, 14th AIAA Applied Aerodynamics Conference, New Orleans, LA, June 1996.

[42]Ciffone, D. L., and Orloff, K. L., "Far-Field Wake-Vortex Characteristics of Wings," *Journal of Aircraft*, Vol. 12, No. 5, May 1975, pp. 464–470.

[43]Corsiglia, V. R., Schwind, R. G., and Chigier, N. A., "Rapid Scanning, Three Dimensional Hot Wire Anemometer Surveys of Wing-Tip Vortices," NASA CR-2180, 1973.

[44]McCormick, B. W., Tangler, J. L., and Sherrieb, H. E., "Structure of Trailing Vortices," *Journal of Aircraft*, Vol. 5, No. 3, July 1968, pp. 260–267.

[45]Kraft, C. C., "Flight Measurements of The Velocity Distribution and Persistence of the Trailing Vortices of an Airplane," NACA TN 3377, 1955.

[46]Rose, R., and Dee, W. F., "Airfract Vortex Wake and Their Effects on Aircraft," Aeronautical Research Council Report No. CP-795, 1965.

[47]Ananthan, S., Leishman, J. G., and Ramasamy, M., "The Role of Filament Stretching in the Free-Vortex Modeling of Rotor Wakes," American Helicopter Society 58th Annual National Forum, Montréal, Canada, June 11–13, 2002.

[48]Takahashi, R. K., and McAlister, K. W., "Preliminary Study of a Wing-Tip Vortex Using Laser Velocimetry," NASA TM 88343, January 1987.

[49]McAlister, K. W., Sculer, C. A., Branum, L., and Wu, J. C., "3-D Wake Measurements Near a Hovering Rotor for Determining Profile and Induced Drag," NASA TP 3577, 1995.

[50]Thompson, T. L., Komerath, N. M., and Gray, R. B., "Visualization and Measurement of the Tip Vortex Core of a Rotor Blade in Hover," *Journal of Aircraft*, Vol. 25, No. 12, December 1988, pp. 1113–1121.

[51]Sullivan, J. P., "An Experimental Investigation of Vortex Rings and Helicopter Rotor Wakes Using a Laser Doppler Velocimeter," Massachusetts Institute of Technology Aerophysics Laboratory Technical Report 183, MIT DSR No. 80038, June 1973.